We are IntechOpen,
the world's leading publisher of
Open Access books
Built by scientists, for scientists

5,600
Open access books available

137,000
International authors and editors

170M
Downloads

154
Countries delivered to

Our authors are among the

TOP 1%
most cited scientists

12.2%
Contributors from top 500 universities

BOOK CITATION INDEX
CLARIVATE ANALYTICS
INDEXED

WEB OF SCIENCE™

Selection of our books indexed in the Book Citation Index
in Web of Science™ Core Collection (BKCI)

Interested in publishing with us?
Contact book.department@intechopen.com

Numbers displayed above are based on latest data collected.
For more information visit www.intechopen.com

Chapter

Hot Corrosion and Oxidation Behaviour of TiAl Alloys during Fabrication by Laser Powder Bed Additive Manufacturing Process

Ntebogeng Mogale, Wallace Matizamhuka and Prince Cobbinah

Abstract

This research paper summarises the practical relevance of additive manufacturing with particular attention to the latest laser powder bed fusion (L-PBF) technology. L-PBF is a promising processing technique, integrating intelligent and advanced manufacturing systems for aerospace gas turbine components. Some of the added benefits of implementing such technologies compared to traditional processing methods include the freedom to customise high complexity components and rapid prototyping. Titanium aluminide (TiAl) alloys used in harsh environmental settings of turbomachinery, such as low-pressure turbine blades, have gained much interest. TiAl alloys are deemed by researchers as replacement candidates for the heavier Ni-based superalloys due to attractive properties like high strength, creep resistance, excellent resistance to corrosion and wear at elevated temperatures. Several conventional processing technologies such as ingot metallurgy, casting, and solid-state powder sintering can also be utilised to manufacture TiAl alloys employed in high-temperature applications. This chapter focuses on compositional variations, microstructure, and processing of TiAl alloys via L-PBF. Afterward, the hot corrosion aspects of TiAl alloys, including classification, characteristics, mechanisms and preventative measures, are discussed. Oxidation behaviour, kinetics and prevention control measures such as surface and alloy modifications of TiAl alloys at high temperature are assessed. Development trends for improving the hot corrosion and oxidation resistance of TiAl alloys possibly affecting future use of TiAl alloys are identified.

Keywords: titanium aluminides, oxidation, hot corrosion, additive manufacturing, laser powder bed fusion

1. Introduction

Titanium aluminide (TiAl) is a member of group material referred to as intermetallics, consisting of various metals resulting in ordered crystallographic structures formed when the concentration of the alloy exceeds the solubility limit [1]. Properties as low density, high strength and elevated temperature properties

make TiAl replacement candidates for nickel-based superalloys used in the aerospace and automotive industries [2–4]. One such alloy tried and tested by General Electric [5] for commercial turbofan engines is Ti-48Al-2Cr-2Nb. Despite the attractive high-temperature properties attained in research to date, the inherent poor ductility of TiAl at ambient temperatures remains a concern [6]. Over the past 20 years and recently, much work has been devoted to material tailoring through compositional variations and alloying aimed at improving room temperature ductility [7–11].

Phase evolution in TiAl alloys governs the mechanical and physical properties to be obtained. Primarily, two ordered structures exist, namely, γ-TiAl (L1$_0$) and hexagonal α_2-Ti$_3$Al (D0$_{19}$), resulting from different thermo-mechanical treatments. Furthermore, the mechanical properties to be obtained are dependent on the microstructure. Three microstructures exist, namely, equiaxed single γ phase, fully or near (γ/α_2) lamellar and duplex (consisting of colonies of lamellar γ/α_2 and pure γ phase grains). The achieved microstructure is significant for its mechanical properties, especially in structural applications. Duplex microstructures with enhanced ductility measures such as fracture strength, yield strength and strain have been reported [12–14]. Fully lamellar structures, in particular, have shown the best creep performance as contrasted to other microstructural modifications [15–17].

For the intended application, considering the inherent brittle nature of TiAl alloys, material tailoring through microstructural evolution is often necessary. Additionally, the low ductility and brittleness of TiAl alloys at ambient temperatures make their processing using conventional methods difficult. To overcome problems associated with conventional processing, such as microstructural inconsistencies inherited from solidification and phase evolutions resulting in the scattering of mechanical properties, heat treatment cycles are often designed [18–21]. Traditional methods requiring post-treatment are time-consuming, labour and capital intensive, waste a lot of start-up material, and require unnecessary production costs. Therefore, there is a need to manufacture TiAl alloy components without the above-mentioned technical deficiencies and limitations and satisfy industrial needs for component fabrication [22].

For the last decades of the 20th century [23], the Additive Manufacturing (AM) method has been employed to obtain objects by the subsequent material supply. AM mainly aims to complete a collection of traditional subtractive manufacturing practices while avoiding and limiting the need for post mechanical processing such as machining. Laser powder bed fusion (L-PBF) is an AM technique, historically referred to as Selective Laser Melting (SLM) developed by F&S Stereolithographietechnik GmbH with Fraunhofer ILT [24], where a component is manufactured by melting a powder bed in a layer-by-layer sequence employing laser beam irritation [25]. The L-PBF process is initiated by creating a 3D digital part model (usually scan data or a CAD file), followed by slicing the model into thin layers using special software. The powder bed is achieved by spreading powder onto the substrate surface. The powder bed is selectively melted through cross-sectional scanning generated from the 3D part model by applying a laser beam. After cross-section scanning, powder bed layering is achieved by sequentially adding layers one after the other repeatedly until the part is complete. Recent studies [25–29] have shown that L-PBF is an innovative and efficient process employed to manufacture TiAl alloys compared to historically employed traditional manufacturing processes such as casting [30–32], ingot metallurgy [33–35], or even solid-state powder sintering [36–38]. The benefits of L-PBF include short production cycles and cheaper production costs. Also, parts produced are of high quality and have been found to exhibit desirable performance [39].

Exploring AM technologies to improve on properties of TiAl and its alloys is essential. As such, mechanical properties like compressive and tensile ductility

measures [40–42], wear resistance [43, 44], elevated temperature creep and oxidation resistance [45–48] superior to those processed by conventional means have been reported. Operation temperatures in new-generation gas turbines have fast-tracked progress in material development in the aerospace industry.

The dual combination of high temperatures and contaminant-containing aircraft environments shifts focus to hot corrosion and oxidation. Hot corrosion and oxidation can lead to catastrophic failures through material consumption at an unpredictably rapid rate. Much work has been devoted to understanding the hot corrosion and oxidation of TiAl alloys already [49–53]. As such, this research paper serves as a summary of the laser additive manufacturing of TiAl alloys. Particular attention is also given to the mechanisms, kinetics, prevention control and recent developments in hot corrosion and oxidation of TiAl alloys.

2. Titanium aluminide (TiAl) alloys: phase, microstructures and mechanical properties

2.1 Phase and microstructural evolutions

2.1.1 Phase evolutions

The three main phases of the Ti-Al system consist of various TiAl compounds, namely, γ-TiAl, α_2-Ti$_3$Al and TiAl$_3$ [1]. Of the three phases, only γ-TiAl and α_2-Ti$_3$Al have shown to be of engineering significance [54] with outstanding properties. They are lightweight and can be implemented for structural parts, automotive and elevated temperature aerospace applications. The γ-TiAl phase is a face-centred tetragonal ordered phase with an L1$_0$ structure. It consists of atomic layers at 90° to the c-axis [55] with lattice parameters a = 0.4005 nm, c = 0.4070 nm and a tetragonality ratio (c/a) of 1.02 [56, 57]. The compositional range of the γ-TiAl phase is from 48.5 to 66.0 at.% of Al. The α_2-Ti$_3$Al phase has a hexagonal DO$_{19}$ structure with a compositional range from 20 to 38.2 at.% of Al.

The α_2-phase has high hydrogen and oxygen absorption rates and suffers from severe embrittlement, though it exhibits optimum high-temperature strength. The γ-phase has low gaseous absorption rates, outstanding oxidation resistance and poor room-temperature ductility. To maximise engineering benefits, dual-phase TiAl alloys consisting of γ + α_2 phase are used. These alloys show excellent ductility [13, 58] at room temperatures due to the availability of refined lamellar colonies aiding γ-phase deformation [54, 59, 60]. The most known dual TiAl alloys with outstanding tensile properties are referred to as duplex alloys of the nominal (at.%) composition of Ti-(46–49) Al.

2.1.2 Microstructure-mechanical property relations

The four significant microstructures which may result in a Ti-Al system are namely, duplex (DP), near-gamma (NG), nearly lamellar (NL) and fully lamellar (FL). The obtained microstructures are greatly dependent on the processing route, Al compositional variations and thermo-mechanical treatments employed. Of the four, only fully lamellar and duplex have been considered necessary in engineering applications [54]. The evolutions (in **Figure 1**) of the microstructures mentioned above were be summarised in works by Cobbinah et al. [6] and Clemens et al. [61].

NG microstructures are obtained via thermal treatments slightly above the eutectoid temperature (T$_{eu}$), while DP microstructures are achieved between T$_{eu}$ and α-transus temperatures. The thermal treatment implemented significantly
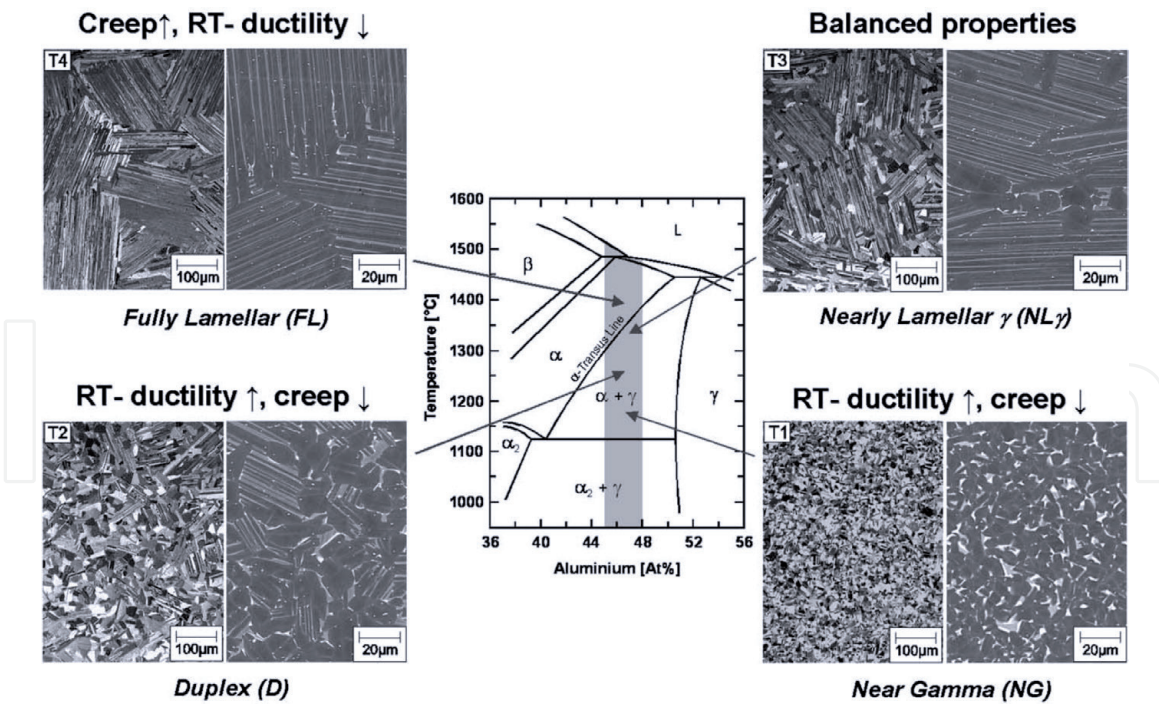
Figure 1.
The central portion of the binary Ti-Al phase diagram together with microscopic optical (left) and backscattered scanning electron (right) images showing NG, DP, NL/NLγ and FL microstructures achieved via heat-treating within α and (α + γ) phase-field. The phases obtained are identified using contrast, where a light contrast is representative of α₂-Ti₃Al and γ-TiAl of a darker contrast [61].

affects the volume fraction of lamellar grains present. As a result, NL microstructures are obtained at (T_{eu}) and T_α relative temperatures, slightly under T_α. NL microstructures exhibiting a specified globular γ-grain volume fraction are shown as NLγ. FL microstructures are achieved by thermal treatments above T_α. Generally, the obtained properties compensate for other properties [22] as represented in **Figure 1** and should be considered when the material is designed for structural applications. Furthermore, the microstructure-property relationship in TiAl alloys makes it easier to modify the material for the anticipated application.

3. Additive manufacturing (AM) of TiAl

3.1 Process overview

Additive manufacturing (AM) presents an opportunity to manufacture TiAl alloys with minimal processing difficulties compared to those experienced during conventional processing, such as near-net-shape forging or investment casting [62]. For tailoring TiAl alloys with optimum properties, laser powder bed fusion (L-PBF) and electron beam melting have been considered suitable [63–66]. Recently, the production of TiAl alloys using L-PBF has gained special attention [29, 67–71] owing to the benefits offered. Some of these benefits [6] complex geometry formation, ease of part dimension control, production of highly defined parts with orifices, mass customisation and material flexibility. Furthermore, during local melting of the powders, high solidification rates are obtained. These result in more refined microstructures.

The component is manufactured (in **Figure 2**) by melting a powder bed in a layer-by-layer sequence employing laser beam irritation [25]. The process is initiated by creating a 3D digital part model (usually scan data or a CAD file), followed by slicing the model into thin layers using special software. The powder bed is achieved by spreading powder onto the substrate surface. In preparation for part
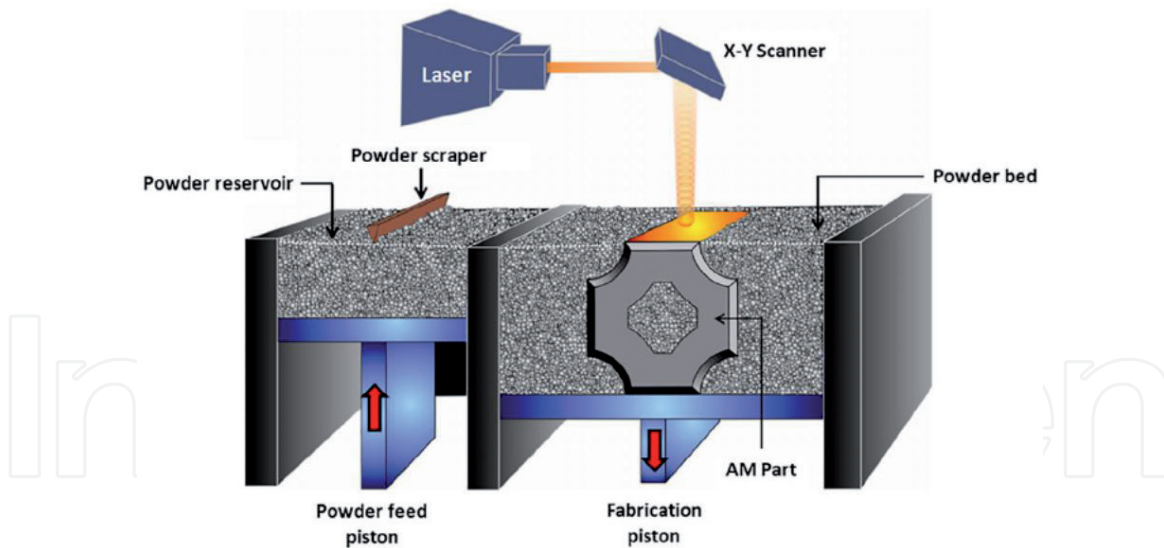
Figure 2.
Graphical representation of laser powder bed fusion method [72].

manufacturing, powders are preheated below their melting temperatures to promote bonding and minimise distortion [6]. L-PBF part manufacturing is executed in an inert gas (preferably argon) sealed environment to prevent reactive powder oxidation.

3.2 Research milestones

The need to replace previously used Ni-based superalloys in aerospace components has fast-tracked research and development of lightweight and cost-efficient TiAl alloys. To date, Ni-based alloys still outmatch TiAl alloys in fabrication costs and mechanical performance. This is mainly due to the poor room temperature ductility of TiAl alloys and the delay in engineering design practices for low ductility materials [54]. Additionally, the high part fabrication costs involved in producing TiAl alloys are related to the knowledge that low ductility fabrication processes, which also produce high melting point alloys, are unavailable. As such, there has been much investment in exploring complex part fabrication techniques, requiring minimal post-processing steps such as L-PBF.

The evidence of many research breakthroughs concerning the production of TiAl alloy parts using L-PBF does not make the processing technique immune to limitations. Efforts have been invested in overcoming processing limitations such as part cracking, micro-pore formation and uneven powder deposition through processing parameter optimisation [73]. Processing parameters can be varied to develop TiAl alloys with excellent mechanical properties in application. Some of these properties are beam size, laser power, scanning speed, scan hatch spacing and powder layer thickness [74].

Polozov et al. [75] confirmed that TiAl-based alloy crack-free samples could be built via L-PBF processing with a high-temperature platform preheating of 900°C. Fully densified samples (highest relative density of 99.9%) were attained at volume energy density 48 J/mm^3. The refined microstructure consisted of equiaxed grains, lamellar α_2/γ colonies and retained β-phase. As compared to conventionally produced TiAl alloys, high ultimate compressive strength and strain values were obtained.

Process parameters can be optimised to aid the fabrication of TiAl specimen, and unfortunately, the resultant part still shows pores, cracks and low densities. One needs to understand the crack and pore formation mechanisms and the defect-process parameter relationships in such a case. Shi and associates [70] investigated

optimal L-PBF process window and the effect of substrate preheating. Moreover, the relationship between crack formation, pore formation, and the process parameters was studied and the crack propagation discrepancy with an increase in the number of deposition layers. It was concluded that crack formation was related to process parameters and the number of deposition layers. The cracks initiated in the 3rd layer are accounted for by residual stress accumulation and the deviations in the composition of Ti-47Al-2Cr-2Nb deposition layers. Furthermore, substrate (Ti-6Al-4 V) preheating at 200°C alleviated cracking. Finally, a good metallurgical bond between the substrate and Ti-47Al-2Cr-2Nb deposition layers was found.

The addition of yttrium (Y) to TiAl alloys (specifically class TNM) and process parameter optimisation dramatically affects the formability, and ultimately the cracking behaviour and control of L-PBF produced components. Gao et al. [76] fabricated TNM alloys with varying Y contents (0, 1, 2, 3, 4 wt.%) and investigated the mechanism of improved formability, cracking sensitivity, cracking behaviour and control mechanism by Y additions. Improvements in the formability of Y added-TNM alloys were assigned to lower melt viscosities and good laser energy absorption. The addition of 2, 3 and 4 wt.% Y to the TNM alloys coupled with a laser energy density greater than 7.00 J/mm^2 formed crack-free samples. The obtained microstructure and phase constituents were reported to contribute to microcrack formation and control significantly. Lower Y additions resulted in coarse columnar grains, oxygen segregation at the grain boundaries with dominating brittle B_2 phase with poor ductility. In contrast, higher Y additions (2–4 wt.%) refined equiaxed grains, enhanced the oxygen-scavenging effect (through the presence of Y_2O_3 particles), and decreased brittle B_2 phase content at higher Y additions significantly improve the ductility.

Finally, adding Nb to γ-TiAl alloys was also reported to account for improved mechanical properties based. Ismaeel et al. [77] produced Ti-Al–Mn–Nb alloys on a TC4 substrate and studied the effects of different Nb contents on the microstructure and properties of the alloys. The phases obtained consisted of γ-TiAl and $α_2$-Ti_3Al and a consecutive microstructural change with increased Nb additions from near full dendrite to near lamellar. Also, adding 7 at.% of Nb resulted in improved alloy's hardness, strength and plastic deformation. Moreover, the elevated temperature oxidation resistance and tribological properties were significantly improved.

4. Hot corrosion

4.1 Definition

Hot corrosion can be defined as a chemical degradation on the metallic surface of materials operating at high temperatures, enhanced by the presence of molten ash and gases containing elements such as sulphur (S), chlorine and sodium [78]. Such environmental elements during fuel combustion promote damage to the protective oxide film by forming contaminants such as V_2O_5 and Na_2SO_4 [79]. This degradation form was initially identified in the early 1950s on combustion engines and boilers [80] and has been explored in numerous research works [50, 81–87].

4.2 Characteristics

Hot corrosion exists as Type I (known as High-Temperature Hot Corrosion) or Type II (Low-Temperature Hot Corrosion), with the former occurring above 800–950°C and the latter at 600–750°C [88, 89]. The occurrence of either attack form is dependent on several parameters such as the composition of the alloy,

contaminant, and gas. Furthermore, other vital parameters are temperature and temperature cycles, erosion processes and gaseous velocity [90, 91]. The main difference between high-temperature hot corrosion (HTHT) and low-temperature hot corrosion (LTHC) is the morphologies thereof. HTHC is distinguished by the occurrence of a non-porous protective scale, internal sulphidisation and chromium (Cr) depletion.

4.2.1 High-temperature hot corrosion (HTHC)-type I

This form of attack, also referred to as molten salt-induced corrosion, comprises a liquid-phase salt mixture deposit observed at high temperatures at the start of deposition [92]. Traditionally, according to Nicholls and Simms [93], HTHC has been detected in a temperature array between the surface deposit melting point and vapour deposition dew point for the deposit. Above this suggested temperature band, instability of dew point deposit exists, resulting in evaporation. A series of chemical reactions occur, initially attacking the oxide film and progress to deplete Cr present in the substrate [94]. Oxidation of the base material is then accelerated by Cr depletion, promoting a porous oxide scale formation.

An example of this could be the formation of thermodynamically unstable liquid sodium sulfate (Na_2SO_4) deposits. The marine environment mainly sources such deposits in sea salt form, followed by atmospheric contaminants such as volcanic discharges and fuel. During combustion, the present Na_2SO_4 can combine with pollutants present in air or fuel (such as chlorides, V and Pb) to form a blend of low melting temperature salts, further broadening the temperature range attack [94]. In the presence of sodium chloride (NaCl), the following reaction after combustion can be observed:

$$2NaCl + SO_2 + O_2 = Na_2SO_4 + Cl_2 \qquad (1)$$
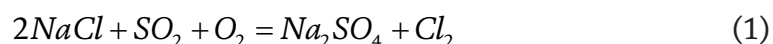
HTHC can be classified into four stages from initiation up to failure [95]:

1. Stage I: Initial coating deterioration—roughening of the surface edges coupled with localised oxide layer disintegration and minor base metal layer depletion is observed. If the surface is left untreated, the condition will worsen. Surface recoating and stripping may be adequate to remedy this degree of damage.

2. Stage II: Oxide layer rapture—characterised by an acceleration and advancement in surface roughness compared to Stage 1 and the protective oxide layer's failure. Although the mechanical integrity remains maintained, there is no way to salvage the component to its original state.

3. Stage III: Detrimental sulphidisation—depicted by massive scale build-up on the component's surface and indications of liquid Na_2SO_4 under the protective layer. The structural integrity of the part is significantly affected, attack by S contaminants proceeds.

4. Stage IV: Catastrophic attack—failure of the component occurs due to the observed significant blistered scale penetrating much into the base metal. Structural rigidity is lost.

This corrosion damage is characterised by a uniform attack, internal sulphide phases, depletion zone beneath a relatively smooth scale–metal interface [80, 96].

4.2.2 Low-temperature hot corrosion (LTHC)-type II

Type II corrosion has been reported [97–102] as a liquid-phase deterioration by a blend of molten nickel (Ni) or cobalt (Co)-containing sulphates such as Na_2SO_4-$CoSO_4$ or Na_2SO_4-$NiSO_4$ accountable for corrosion initiation and propagation. The corrosion initiation is achieved through oxide layer fluxing, while propagation is accelerated by the mass movement of reactive elemental components through liquids present in the corrosion pits [80]. Studies [103–106] have shown that conversion from CoO and NiO occurs when SO_3 in the gas reacts with the sulphates, attributing to the extensive usage of mixed Na_2SO_4-$NiSO_4$ in recent LTHC research studies.

LTHC can be found in coated or uncoated compressor and turbine parts. For instance, the sometimes turbine blade's uncoated internal cooling systems operating at temperatures of about 650–750°C may be prone to this corrosion type [107]. The external rim of uncoated turbine blades reaches temperatures of 400–800°C [108]. LTHC is distinguished by the pit's appearance and the absence of a sulphide zone at the corrosion front, consuming all the S [96].

4.3 Mechanisms

Two HTHC mechanisms have been proposed, namely sulphide-oxidation and salt fluxing mechanisms [94]. Acidic and basic fluxing reactions, presented initially by Goebel and Pettit [109, 110], may be obtained and rely on the compositions of the alloy, oxide and underlying coating [93]. According to this model, fluxing occurs due to the decomposition of oxides into corresponding cations and O^{2-} (known as acidic fluxing) or oxides with O^{2-} forming anions (referred to as basic fluxing).

In acidic fluxing, oxide ions are donated to the deposit melt through dissolving the oxide scale [93]:

$$MO = M^{2+} + O^{2-} \tag{2}$$

Acidic environments in molten deposits can be developed through two main processes, namely, alloy-induced and gas-phase acidic fluxing. Basic fluxing is achieved through the production of oxide ions in a Na_2SO_4 deposit. Such is obtained by removing S and oxygen from the residue through reactions with the alloy or underlying coating. Subsequently, the oxide scales (e.g., MO) produced can react with the oxide ions through reactions [93]:

$$MO + O^{2-} = MO_2^{2-} \tag{3}$$

A conventional model for LTHC was proposed by Luthra [111]. As suggested by the model, LTHC follows two stages, namely, formation of liquid-form sodium-cobalt sulphate and attack propagation through SO_3 migration through the liquid salt. In nickel-based alloys, the mechanism suggested by Shih and associates [112] for LTHC is sulphidisation.

4.4 Laboratory testing techniques

An alloy's resistance to hot corrosion can mainly be determined using four standard tests: the electrochemical, crucible, accelerated oxidation, and burner-rig [94, 113]. The crucible tests remain the most highly ranked test for hot corrosion, simply consisting of either suspending, depositing, or completely immersing the testing sample in molten salts at elevated temperatures, as presented in **Figure 3**. As

far as TiAl alloys are concerned, less work has been carried out to understand the hot corrosion behaviour of such alloys [114–116].

Gas turbine environments can be precisely simulated by employing burner-rig tests [117, 118], shown in **Figure 4**. The salt is in aerosol or fog form and fuel oil/ air is introduced into the testing chamber to generate the test environment [119]. Simmons et al. [120] indicated that hot corrosion is an electrochemical process since hot corrosion consists of electrochemical reactions in which the molten salt acts as the conductive media or electrolyte.

4.5 Prevention methods

Some of the approaches used to prevent hot corrosion include maintaining both fuel purity and composition, properly selecting structural alloys, employing coatings, cleaning hot parts and air filtering [94].

4.5.1 Fuel purity and composition

Initiation and propagation of hot corrosion are greatly affected by impurities such as vanadium (V), S, and various alkali earth metals [121]. This can be controlled by adding magnesium (Mg), Cr, barium and calcium to the combustion fuel
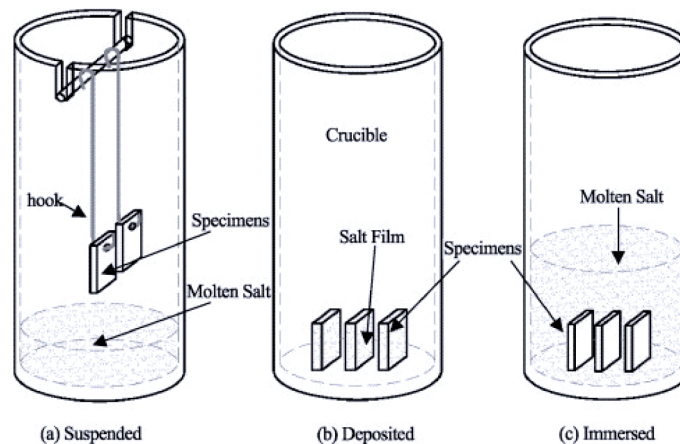

Figure 3.
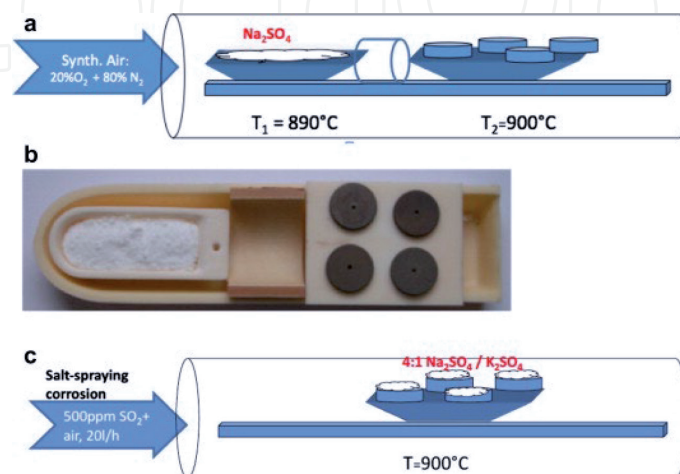*Configurations used in hot corrosion crucible testing [114].*

Figure 4.
Burner rig hot corrosion test schematic representation where (a) is an illustrates the experimental setup for $Na_2SO_4(g)$ exposure, (b) is an image of the specimen plate for $Na_2SO_4(g)$ tests in a crucible with the salt container and (c) is an ex-situ salt hot corrosion schematic diagram setup for experimental studies [119].

to decrease corrosion rate. The presence of zinc (Zn) in the form of anodes in the combustion fuel or as part of the protective coating can significantly reduce the occurrence of LTHC. According to Hancock and associates [122], Zn drastically reacts with chloride ions (i.e., when excess NaCl is available) and transfers the chloride to the gas-salt interface to transform to chloride gas via sulphidisation.

4.5.2 Proper alloy selection

The addition of Cr to superalloys has effectively reduced the occurrence of hot corrosion [123]. Historically [121, 124], Cr (15 wt.% for Ni-based and 25 wt.% for Co-based alloys) has been added to superalloys to reduce HTHC. Much related to TiAl alloys, Garip and Ozdemir [125] studied the effect of Cr, Mo and Mn on the cyclic hot corrosion behaviour, and subsequently reported the beneficial effects of Cr and Mn additions on the hot corrosion properties of the investigated samples. Cr's effect on corrosion resistance is attributed to the ability of Cr to form Cr_2O_3, stabilising the chemistry melt, preventing reprecipitation of the protective oxide scale. Contrarily, increased Cr additions to superalloys can compromise the high-temperature strength and ductility [113] by forming TCP phases. The alloy and oxide film adhesion has been reported to be improved by the addition of zirconium, yttrium, scandium, cerium and lanthanum [113]. Silicon (Si), platinum (Pt), hafnium, Ti, Al, and Nb [126] were also found to increase resistance to hot corrosion.

4.5.3 Protective coatings

Such as diffusion, overlay and thermal barrier (TBCs) coatings can be used on relatively resistant alloys to combat hot corrosion. An alloy's surface enrichment by Al, Si or Cr achieves diffusion coatings. Various aluminide diffusion coatings (i.e., PWA70, MDC3V, PWA62, TEW LDC2, Elbar Elcoat 360 and Chromalloy RT22) have been developed and can be alloyed with Pt to improve cyclic oxidation at high temperatures [127]. Overlay coatings, commonly referred to as M (base metal)–Cr–Al–Y coatings, are designed for LTHC and HTHC surface protection. Overlay coatings with low Cr-high Al coatings are used for HTHC protection, while high Cr-low Al coatings are used for LTHC [94]. TBCs protects the substrate from gaseous flow caused by heat and consist of an external ceramic usually zirconia) and an oxidation-resistant bond-coat overlay. Other coatings include intelligent coatings like RT22 (Pt-aluminide) and Sermetal 1515 (a triple-cycle Si-aluminide treatment), have been reported [127].

Inexpensive alternatives include oxide-based glass and glass–ceramic coatings [128, 129]. Oxide-based glass and glass–ceramic coatings exhibit a remarkable combination of properties such as excellent chemical inertness, high-temperature stability and superior mechanical properties, which effectively can mitigate deterioration caused by hot corrosion. The introduction of halogens on the surface of the alloy encourages the preferential formation of aluminium halides at elevated temperatures. The aluminium halides are then converted to thin, continuous, and protective alumina oxides. Fluorine provides the best oxidation protection [130]. Further examples of surface modifications coating and methods studied on γ-TiAl alloys include magnetron sputtering [131], laser cladding [132], sol–gel [133], pack cementation [134], chemical vapour deposition [135], slurry [136], ion implantation [137].

4.5.4 Cleaning hot parts and air filtering

Motoring washes can be flooded with plain water [121] to prevent hot corrosion using specified procedures in the maintenance manual for the specific engine model. Also, high-efficiency filters can be used to filter out air containing high sodium contents [138].

4.6 Hot corrosion studies for TiAl alloys

Although much work has been devoted to understanding the hot corrosion kinetics of Ni-based and Co-based superalloys, TiAl alloys emerged to have sparked much interest in recent years [1, 56, 57, 139]. Historically, reported works utilised alloys produced using conventional methods; however, more attention has recently shifted to AM routes [70, 73, 140–146]. Despite much devotion to improving structure–property relations of TiAls, little work has been reported on the hot corrosion of additively manufactured TiAl.

Garip and Ozdemir [147] produced an alloy to the nominal at.% composition of Ti-48Al-10Cr using electric current activated sintering and studied the hot corrosion kinetics of the alloys in Na_2SO_4 salt for 180 h at 700–900°C. A severe hot corrosion attack was observed at 900°C (refer to **Figure 5**), with a porous and loose layer consisting of $Na_2Ti_3O_7$, TiO_2, Al_2O_3 traces of TiS phase.

In a study led by Xiong et al. [67], bare alloys TiAl, TiAlNb, and Ti_3AlNb, were severely damaged after exposure at 750°C in $(Na, K)_2SO_4$ + NaCl melts as compared to those coated with enamel or TiAlCr. The corrosion mechanism was described to be much related to self-catalysis of sulphidisation and chlorination of metallic components. The initial mass loss observed is due to chloride volatility via metallic component chlorination. Of the alloys investigated, TiAlNb exhibited the best corrosion resistance due to adhesive Al_2O_3 enriched scale formation. Lastly, the degradation acceleration of sputtered TiAlCr coating was reported to be due to the chlorination of Cr and Al.

Additions of Nb and Si to traditional TiAl coatings were found to improve the hot corrosion resistance of a Ti-6Al-4 V alloy. In the stated work, Dai et al. [148] investigated the corrosion mechanisms on a mass loss basis following exposure at 800°C in a 75 wt.% Na_2SO_4 + NaCl salt mixture. Increasing single Nb additions deteriorated the hot corrosion resistance of the coating. Comparatively, increasing single Si additions continued to improve hot corrosion resistance. However, additions of both Nb and Si simultaneously showed better resistance to corrosion than single element additions. The corrosion protection of both Nb and Si (as seen in **Figure 6**) was related to SiO_2 and Al_2O_3 formation in the initial stages of hot corrosion. Secondly,

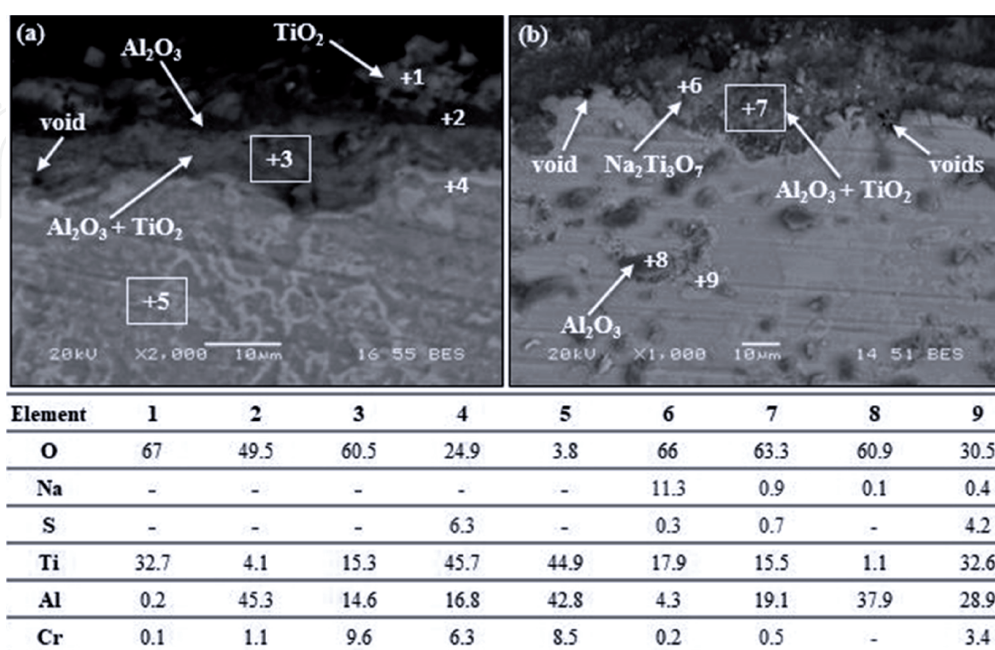| Element	1	2	3	4	5	6	7	8	9
O	67	49.5	60.5	24.9	3.8	66	63.3	60.9	30.5
Na	-	-	-	-	-	11.3	0.9	0.1	0.4
S	-	-	-	6.3	-	0.3	0.7	-	4.2
Ti	32.7	4.1	15.3	45.7	44.9	17.9	15.5	1.1	32.6
Al	0.2	45.3	14.6	16.8	42.8	4.3	19.1	37.9	28.9
Cr	0.1	1.1	9.6	6.3	8.5	0.2	0.5	-	3.4

Figure 5.
Cross-sectional SEM images showing oxide scale microstructures with EDS analysis points represented in at.%, after hot corrosion exposure at (a) 800°C and (b) 900°C for 180 h [147].
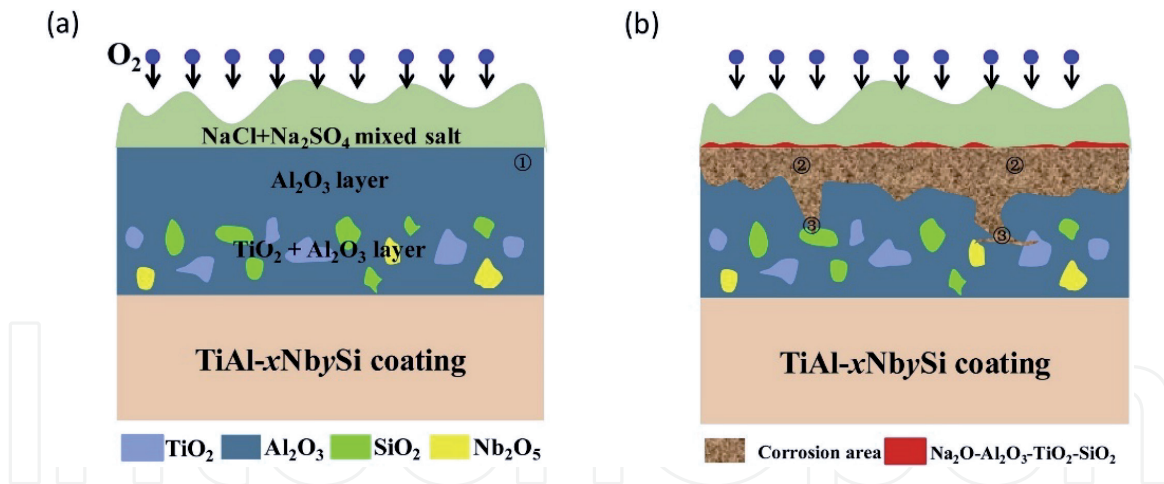
Figure 6.
Representative hot corrosion model of TiAl-xNbySi coating where (a) illustrates TiO₂ and Al₂O₃ formation and (b) shows an acidic dissolution of TiO₂ to form sodium titanates including NaTiO₂ and Na₂TiO₃ [148].

Si additions were reported to promote the formation of a Na_2O-Al_2O_3-TiO_2-SiO_2 enamel, hindering contact between the corrosive media and the oxide scales.

Tang et al. [149] studied the effect of enamel coatings on γ-TiAl against hot corrosion at 900°C. The enamel coating remained stable in the $(Na,K)_2SO_4$ melts, thus effectively protecting it against hot corrosion attack. Silicon-based coatings have also been shown to protect TiAl alloys. Rubacha et al. [150] evaluated the hot corrosion resistance of silicon-rich coated Ti-46Al-8Ta (at.%) alloy in NaCl, Na_2SO_4 and a mixture of the two salts. The formation of an amorphous SiO2 layer with TiO2 (rutile) and α cristobalite crystals enhanced the hot corrosion resistance of the TiAl alloy. Furthermore, Wu and colleagues [151] studied the hot corrosion resistance of a SiO_2 coated TiAl alloy in 75 wt.% Na_2SO_4 + 25 wt.% NaCl salt mixture at 700°C. The enhanced hot corrosion resistance of the TiAl alloy was attributed to the formation of a compact and adherent amorphous SiO_2 embedded with $Na_2Si_4O_9$ and cristobalite. The incorporation of Si in aluminide coatings has also provided long-term oxidation protection of γ-TiAl alloys at temperatures of 950°C by forming a continuous and uniform α-alumina oxide scale [152].
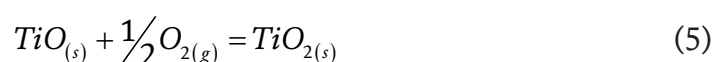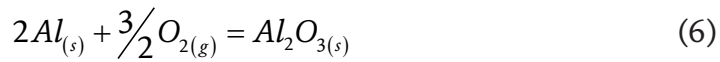
5. Oxidation

5.1 Definition

When metallic materials are exposed to elevated temperatures in air, oxidation occurs, resulting in the formation of oxide scales. The crystal structure of the individual metals significantly affects the oxidation rate of high-temperature applicative parts [153, 154].

5.2 Oxidation behaviour in TiAl alloys

The following reactions may occur when TiAl alloys are subject to an oxidising environment:

$$\frac{1}{2}Ti_{(s)} + O_{2(g)} = TiO_{(s)} \tag{4}$$

$$TiO_{(s)} + \frac{1}{2}O_{2(g)} = TiO_{2(s)} \tag{5}$$

$$2Al_{(s)} + \frac{3}{2}O_{2(g)} = Al_2O_{3(s)} \qquad (6)$$

The ultimate oxidation resistance of alloyed TiAls is achieved by forming protective Al_2O_3, Cr_2O_3 and SiO_2 scales due to their outstanding thermal stabilities. In contrast, the unfavourable formation of porous TiO_2 with a high crack tendency is often observed [153]. Cobbinah et al. [155] found that 4 and 8 at.% Ta additions to Ti-46.5Al alloy promoted the significant formation of a consistent, non-porous Al_2O_3 layer at the metal-oxide boundary. Additionally, the layer operated as a diffusion barrier and preceded to outstanding oxidation resistance of the TiAl alloys.

In a study by Pan et al. [156], a comprehensive understanding is provided of the role of alloying on the oxidation resistance of TiAl alloys. Protection was related much to the formation of Ti_3Sn layer diminishing oxygen diffusion inwardly, promoted by Sn additions. Moreover, spallation resistance was enhanced by the Al_2O_3 oxide pegs providing a mechanical locking. The effect of cathodically electrodepositing a SiO_2 film on the oxidation resistance of a TiAl alloy was studied [157]. After 900°C exposure in air, the resultant alumina- and silicon-enriched glass-like oxide scale (in **Figure 7**) was reported, preventing oxygen diffusion leading to remarkably decreased alloy oxidation rates.

Surface modification of TiAl alloys via anodising has sparked interest in many high-temperature oxidation studies [158–161]. For instance, the oxidation behaviour and protection mechanisms of a TiAl alloy were studied by anodising in a methanol/NaF solution and produced an aluminium (Al)-and fluorine-enriched anodic film [162]. After 100 h exposure at 850°C, no evidence of cracking and spallation was displayed on the surface. The enhanced high-temperature oxidation resistance is mainly attributed to the halogen effect, generation of Al_2O_3 and oxidised Al–F species inhibiting external oxygen diffusion. Much effort has been devoted to developing coatings for γ-TiAl alloys, summarised in an evaluation by Pflumm et al. [130]. Amongst many available coating methods, Si-modified aluminide coatings produced via pack cementation have gained popularity. One such study [81] demonstrated that a continuous α-Al_2O_3 scale remained adherent after exposure to a temperature of 950°C for 3000 h.

5.3 Oxidation kinetics of TiAl alloys

When a metal operating at elevated temperatures is exposed to air, an oxide scale forms. As oxide scale formation proceeds, the metal's weight change can be plotted against time. Several laws such as linear, parabolic, logarithmic or cubic can be observed when studying oxidation kinetics [163]. In as far as TiAl alloys are

Figure 7.
Representation of a γ-TiAl alloy coated with E-SiO₂ film (a) and after thermal oxidation test (b) [157].

concerned, either linear or parabolic oxidation kinetics prevail. While the former offers no protection against high-temperature oxidation, the latter promotes diffusion-controlled oxide scale formation, improving much on the oxidation resistance of the base material. Parabolic oxidation follows and obeys the following law:

$$\left(\Delta m \middle/ A\right)^2 = k_p t \tag{7}$$

where Δm = change in weight (in mg), A = surface area (in cm^2), t = time (in sec) and k_p = parabolic oxidation rate constant (in mg^2.cm^{-4}.sec^1).

The optimum oxidation protection governed by the parabolic law often results in a thick and continuous TiO$_2$ and Al$_2$O$_3$ scale. As such, Swadźba et al. [48] investigated the short-term oxidation behaviour of a TiAl 48–2-2 alloy produced by AM at a temperature range of 750–900°C in air. At 900°C, a non-porous scale consisting of TiO$_2$, Al$_2$O$_3$ and nitrates, exhibiting parabolic oxidation (in **Figure 8**), was observed.

Garip [164] likewise studied the oxidation kinetics at 900°C in air for 200 h for TiAl alloys produced via pressureless and resistance sintering. Both alloys exhibited a nearly parabolic oxidation response, with oxidation rate constants of the pressureless sintered alloy of 0.6391 mg^n cm^{-2n} h^{-1}, 1.8 times higher than that of the alloy compacted using resistance sintering. Multi-layered oxide scales consisting of TiO$_2$ and Al$_2$O$_3$ were obtained.
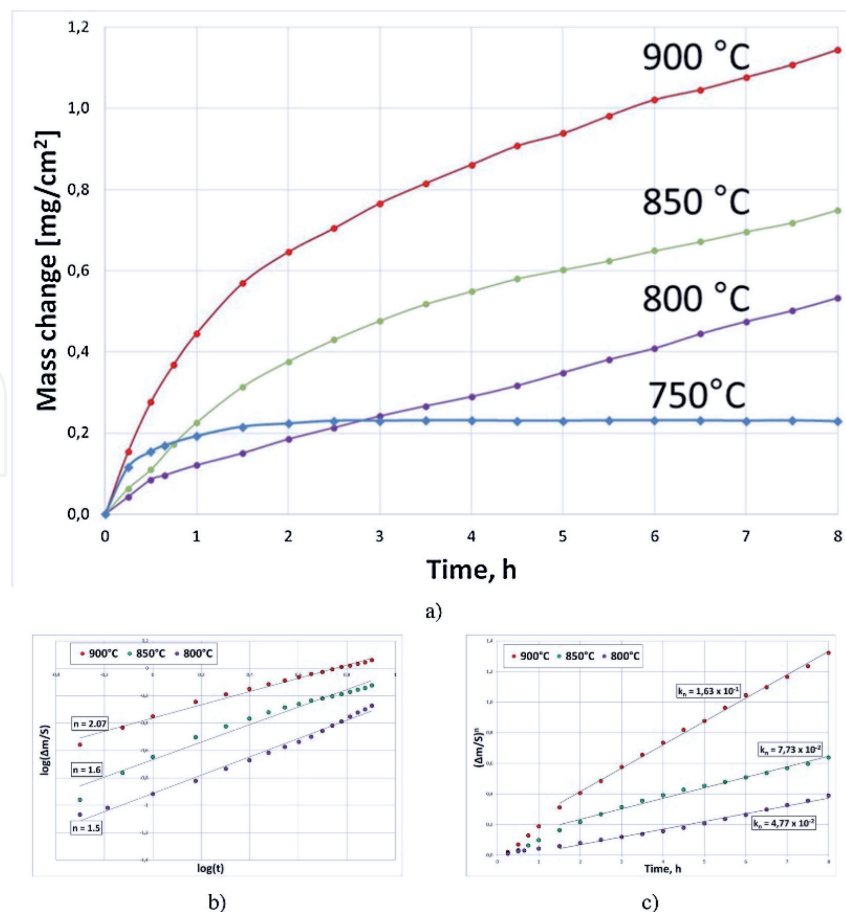

Figure 8.
Mass change against time plots for (a) oxidation rate constant of the AM produced TiAl 48–2-2 alloy and (b)–(c) the power-law constant – n extrapolation [48].

5.4 Effect of alloy modifications on the oxidation resistance of TiAl

Oxidation protection offered by forming a continuous Al_2O_3 scale followed by a multilayer of $TiO_2 + Al_2O_3$ is limited, unfortunately, to the maximum service temperature of ~830°C. Above this temperature, the protection potential presented by the oxide scales formed severely deteriorates, limiting the high-temperature application potential for structural components [165]. The current trend in research is to improve the oxidation resistance of TiAl through alloy modifications.

Nb is one element used in many research works [86–90] to improve the oxidation resistance of TiAl alloys. Al activities are promoted by Nb additions and accelerate protective Al_2O_3 oxide film formation, limiting oxygen diffusion into the alloy [166]. Also, the α_2 phase present in TiAl alloys is significantly decreased by Nb additions, decreasing its oxygen solubility [54]. Although Nb was primarily used for improving oxidation resistance [167], other high-temperature properties such as strength and creep resistance have been enhanced by the presence of Nb.

The creep resistance and the oxidation resistance of TiAl and its alloys can be enhanced by adding Si. The oxidation improvement is said to be achieved through the refinement of TiO_2 particles, inducing refined and compact TiO_2 scales on the surface [165]. Moreover, Si promotes Al diffusion into the oxide scale, stabilises Ti, reduces Ti^{4+} ions and impedes external Ti^{4+} ions diffusion [168].

The effect of adding molybdenum (Mo) alone to TiAls to improve on high-temperature oxidation is minimal. The protection of Mo-containing TiAl alloys is through the formation of inner oxide layers of TiO_2 and Ti_2AlMo near the substrate surface [165]. Unfortunately, Mo additions cannot alter the external oxide film formed (i.e., comprises of loose and porous TiO_2 scales) and its characteristics. It is recommended in practice that the improvement of high-temperature oxidation cannot be derived from adding Mo alone; instead, the combination of Mo with other alloys can have a beneficial effect on the alloys' resistance to oxidation [169].

Cr additions promote the formation of Cr_2O_3 oxides, which act as mass ion transport barriers [170], enhancing oxidation resistance. In addition, the Al content existing in the alloys can be significantly suppressed by Cr additions, promoting the formation of Al_2O_3 scales. Oxygen diffusion at elevated temperatures can be accelerated by Cr^{3+} ion doping in titanium oxide, improving oxygen vacancy concentration. Contrarily, the doping effect may impair the TiAl alloy's oxidation by making Ti^{4+} interstitially occupying TiO_2 sites, improving the potential energy with a noticeable decrease in diffusion activation energy, encouraging the diffusion of Ti^{4+} in TiO_2 [171].

Zirconium (Zr) additions can also enhance oxidation properties by altering the characteristics of the oxide formed during the primary stages of oxidation and promote oxide grain nucleation [172]. As a result, the refinement of the oxide particles occurs, which can hinder oxygen diffusion. Rare earth metals have been reported to enhance the oxidation resistance of TiAl alloys. As discussed in detail in a research paper by Dai et al. [165], the protection mechanism is contributed by grain refinement, substrate purification, oxide adherence improvement and promotion of Al selective oxidation.

6. Conclusions

The need for materials to give excellent mechanical properties under high temperatures and extreme conditions such as TiAl is in demand. The use of such alloys would mean a reduction in pollution and noise levels for aero-based engines due to improved thermal efficiencies. There are challenges in producing such alloys using

the conventional arc and induction melt casting techniques due to the extremely high melting temperatures of the alloys. The AM route, particularly L-PBF, presents an opportunity to produce such alloys. What is critical in such trials is the operating parameters during processing. This has a direct influence on the performance and mechanical properties of the alloys so produced. Hot corrosion and oxidation of TiAl alloys are of great concern in gas turbine engines. Hot corrosion can be classified into HTHC and LTHC, with particular reference to mechanisms and characteristics. Protection control methods may result in fewer catastrophic failures. The hot corrosion process must be either totally prevented or detected early to avoid catastrophic failure. A sound understanding of oxidation mechanisms and kinetics of TiAl alloys makes it easier to tailor oxidation-resistant alloys by alloy modifications.

Acknowledgements

Conflict of interest

The authors declare no conflict of interest.

Author details

Ntebogeng Mogale*, Wallace Matizamhuka and Prince Cobbinah
Vaal University of Technology, Johannesburg, South Africa

*Address all correspondence to: ntebogeng.mogale@yahoo.co.za

IntechOpen

References

[1] Mphahlele MR, Olevsky EA, Olubambi PA. Chapter 12—Spark plasma sintering of near net shape titanium aluminide: A review [Internet]. Cao G, Estournès C, Garay J, Orrù R, editors. Spark Plasma Sintering. Elsevier; 2019. p. 281-299. Available from: http://www.sciencedirect.com/science/article/pii/B978012817744000012X

[2] Reith M, Franke M, Schloffer M, Körner C. Processing 4th generation titanium aluminides via electron beam based additive manufacturing—Characterization of microstructure and mechanical properties. Materialia [Internet]. 2020;14:100902. Available from: https://www.sciencedirect.com/science/article/pii/S2589152920303185

[3] Bewlay BP, Nag S, Suzuki A, Weimer MJ. TiAl alloys in commercial aircraft engines. Mater High Temp. 2016;33(4-5):549-559.

[4] Clemens H, Smarsly W. Light-weight intermetallic titanium aluminides—Status of research and development. In: Advanced materials research. Trans Tech Publ; 2011. p. 551-556.

[5] Kim Y-K, Hong JK, Lee K-A. Enhancing the creep resistance of electron beam melted gamma Ti–48Al–2Cr–2Nb alloy by using two-step heat treatment. Intermetallics [Internet]. 2020;121:106771. Available from: https://www.sciencedirect.com/science/article/pii/S0966979519312014

[6] Cobbinah PV, Nzeukou RA, Onawale OT, Matizamhuka WR. Laser Powder Bed Fusion of Potential Superalloys: A Review. Metals (Basel) [Internet]. 2020 Dec 30 [cited 2021 Feb 5];11(1):58. Available from: https://www.mdpi.com/2075-4701/11/1/58

[7] Cui N, Wu Q, Yan Z, Zhou H, Wang X. The Microstructural Evolution, Tensile Properties, and Phase Hardness

of a TiAl Alloy with a High Content of the β Phase. Materials (Basel) [Internet]. 2019 Aug 28 [cited 2021 Feb 5];12(17):2757. Available from: https://www.mdpi.com/1996-1944/12/17/2757

[8] Li J, Jeffs S, Whittaker M, Martin N. Boride formation behaviour and their effect on tensile ductility in cast TiAl-based alloys. Mater Des. 2020 Oct 1;195:109064.

[9] Liu H, Li Z, Gao F, Liu Y, Wang Q. High tensile ductility and strength in the Ti-42Al-6V-1Cr alloy. J Alloys Compd. 2017 Mar 25;698:898-905.

[10] Shu S-L, Tong C-Z, Qiu F, Zou Q, Jiang Q-C. Effects of ternary elements on the ductility of TiAl. Can Metall Q [Internet]. 2016 Apr 2 [cited 2021 Feb 5];55(2):156-60. Available from: http://www.tandfonline.com/doi/full/10.1080/00084433.2016.1169660

[11] Huang S-C, Hall EL. The effects of Cr additions to binary TiAl-base alloys. Metall Trans A. 1991;22(11):2619-2627.

[12] Gu X, Cao F, Liu N, Zhang G, Yang D, Shen H, et al. Microstructural evolution and mechanical properties of a high yttrium containing TiAl based alloy densified by spark plasma sintering. J Alloys Compd. 2020 Apr 5;819:153264.

[13] Zhou H, Kong F, Wang X, Chen Y. High strength in high Nb containing TiAl alloy sheet with fine duplex microstructure produced by hot pack rolling. J Alloys Compd. 2017 Feb 25;695:3495-3502.

[14] Zhao ET, Niu HZ, Zhang SZ, Feng L, Yang SY. Microstructural control and mechanical properties of a β-solidified γ-TiAl alloy Ti-46Al-2Nb-1.5V-1Mo-Y. Mater Sci Eng A. 2017 Jul 31;701:1-6.

[15] Burtscher M, Klein T, Mayer S, Clemens H, Fischer FD. The creep behavior of a fully lamellar γ-TiAl based alloy. Intermetallics. 2019 Nov 1;114:106611.

[16] Ding R, Chiu Y, Chu M, Paddea S, Su G. A study of fracture behaviour of gamma lamella using the notched TiAl micro-cantilever. Philos Mag [Internet]. 2020 Apr 17;100(8):982-97. Available from: https://doi.org/10.1080/14786435.2020.1714088

[17] Wimler D, Lindemann J, Clemens H, Mayer S. Microstructural Evolution and Mechanical Properties of an Advanced γ-TiAl Based Alloy Processed by Spark Plasma Sintering. Materials (Basel). 2019;12(9):1523.

[18] Cui N, Wu Q, Bi K, Xu T, Kong F. Effect of heat treatment on microstructures and mechanical properties of a novel β-solidifying TiAl alloy. Materials (Basel). 2019;12(10):1672.

[19] Chlupová A, Heczko M, Obrtlík K, Dlouhý A, Kruml T. Effect of heat-treatment on the microstructure and fatigue properties of lamellar γ-TiAl alloyed with Nb, Mo and/or C. Mater Sci Eng A. 2020 Jun 1;786:139427.

[20] Chen L, Zhu L, Guan Y, Zhang B, Li J. Tougher TiAl alloy via integration of hot isostatic pressing and heat treatment. Mater Sci Eng A. 2017 Mar 14;688:371-377.

[21] Stendal JA, Eisentraut M, Imran M, Sizova I, Bolz S, Weiß S, et al. Accelerated hot deformation and heat treatment of the TiAl alloy TNM-B1 for enhanced hot workability and controlled damage. J Mater Process Technol. 2021 May 1;291:116999.

[22] Mphahlele MR, Olevsky EA, Olubambi PA. Spark plasma sintering of near net shape titanium aluminide:

A review. In: Spark Plasma Sintering. Elsevier; 2019. p. 281-299.

[23] Campbell I, Diegel O, Kowen J, Wohlers T. Wohlers report 2018: 3D printing and additive manufacturing state of the industry: annual worldwide progress report. Wohlers Associates; 2018.

[24] Yap CY, Chua CK, Dong ZL, Liu ZH, Zhang DQ, Loh LE, et al. Review of selective laser melting: Materials and applications. Appl Phys Rev [Internet]. 2015 Dec 1;2(4):41101. Available from: https://doi.org/10.1063/1.4935926

[25] Doubenskaia M, Domashenkov A, Smurov I, Petrovskiy P. Study of Selective Laser Melting of intermetallic TiAl powder using integral analysis. Int J Mach Tools Manuf. 2018 Jun 1;129:1-14.

[26] ISMAEEL A, WANG C shan. Effect of Nb additions on microstructure and properties of γ-TiAl based alloys fabricated by selective laser melting. Trans Nonferrous Met Soc China (English Ed. 2019 May 1;29(5):1007-16.

[27] Kenel C, Dasargyri G, Bauer T, Colella A, Spierings AB, Leinenbach C, et al. Selective laser melting of an oxide dispersion strengthened (ODS) γ-TiAl alloy towards production of complex structures. Mater Des. 2017 Nov 15;134:81-90.

[28] Gussone J, Garces G, Haubrich J, Stark A, Hagedorn YC, Schell N, et al. Microstructure stability of γ-TiAl produced by selective laser melting. Scr Mater. 2017 Mar 15;130:110-113.

[29] Zhou YH, Lin SF, Hou YH, Wang DW, Zhou P, Han PL, et al. Layered surface structure of gas-atomized high Nb-containing TiAl powder and its impact on laser energy absorption for selective laser melting. Appl Surf Sci. 2018 May 31;441:210-217.

[30] Fu PX, Kang XH, Ma YC, Liu K, Li DZ, Li YY. Centrifugal casting of TiAl exhaust valves. Intermetallics. 2008 Feb 1;16(2):130-138.

[31] Aguilar J, Schievenbusch A, Kättlitz O. Investment casting technology for production of TiAl low pressure turbine blades—Process engineering and parameter analysis. Intermetallics. 2011 Jun 1;19(6):757-761.

[32] Liu K, Ma YC, Gao M, Rao GB, Li YY, Wei K, et al. Single step centrifugal casting TiAl automotive valves. In: Intermetallics. Elsevier; 2005. p. 925-928.

[33] Paul JDH, Lorenz U, Oehring M, Appel F. Up-scaling the size of TiAl components made via ingot metallurgy. Intermetallics. 2013 Jan 1;32:318-328.

[34] Zhang J, Jing Y, Fu M, Gao F. Microstructure optimization of ingot metallurgy TiAl. Intermetallics. 2012 Aug 1;27:21-25.

[35] Wang YH, Lin JP, Xu XJ, He YH, Wang YL, Chen GL. Effect of fabrication process on microstructure of high Nb containing TiAl alloy. J Alloys Compd. 2008 Jun 30;458(1-2):313-317.

[36] Trzaska Z, Couret A, Monchoux JP. Spark plasma sintering mechanisms at the necks between TiAl powder particles. Acta Mater. 2016 Oct 1;118:100-108.

[37] Kulkarni KN, Sun Y, Sachdev AK, Lavernia E. Field-activated sintering of blended elemental γ-TiAl powder compacts: Porosity analysis and growth kinetics of Al3Ti. Scr Mater. 2013 Jun 1;68(11):841-844.

[38] Wenbin F, Lianxi H, Wenxiong H, Erde W, Xiaoqing L. Microstructure and properties of a TiAl alloy prepared by mechanical milling and subsequent reactive sintering. Mater Sci Eng A. 2005 Aug 25;403(1-2):186-190.

[39] Gunasekaran J, Sevvel P, John Solomon I. Metallic materials fabrication by selective laser melting: A review. Mater Today Proc. 2020 Jun 3;

[40] Gao B, Peng H, Liang Y, Lin J, Chen B. Electron beam melted TiC/high Nb–TiAl nanocomposite: Microstructure and mechanical property. Mater Sci Eng A. 2021 Apr 15;811:141059.

[41] Todai M, Nakano T, Liu T, Yasuda HY, Hagihara K, Cho K, et al. Effect of building direction on the microstructure and tensile properties of Ti-48Al-2Cr-2Nb alloy additively manufactured by electron beam melting. Addit Manuf. 2017 Jan 1;13:61-70.

[42] Mohammad A, Alahmari A, Mohammed M, Renganayagalu R, Moiduddin K. Effect of Energy Input on Microstructure and Mechanical Properties of Titanium Aluminide Alloy Fabricated by the Additive Manufacturing Process of Electron Beam Melting. Materials (Basel) [Internet]. 2017 Feb 21 [cited 2021 Jul 13];10(2):211. Available from: http://www.mdpi.com/1996-1944/10/2/211

[43] Pradeep GVK, Duraiselvam Muthukannan, Katakam, Prasad S, Mohammad Ashfaq. Tribological Behavior of Additive Manufactured c-TiAl by Electron Beam Melting. Trans Indian Inst Met [Internet]. 1950;73. Available from: https://doi.org/10.1007/s12666-020-01950-8

[44] Xu Z, Ouyang W, Liu Y, Jiao J, Liu Y, Zhang W. Effects of laser polishing on surface morphology and mechanical properties of additive manufactured TiAl components. J Manuf Process. 2021 May 1;65:51-59.

[45] Kim YK, Hong JK, Lee KA. Enhancing the creep resistance of electron beam melted gamma Ti–48Al–2Cr–2Nb alloy by using two-step heat

treatment. Intermetallics. 2020 Jun 1;121:106771.

[46] Kim YK, Youn SJ, Kim SW, Hong J, Lee KA. High-temperature creep behavior of gamma Ti-48Al-2Cr-2Nb alloy additively manufactured by electron beam melting. Mater Sci Eng A. 2019 Aug 19;763:138138.

[47] Kastenhuber M, Klein T, Clemens H, Mayer S. Tailoring microstructure and chemical composition of advanced γ-TiAl based alloys for improved creep resistance. Intermetallics. 2018 Jun 1;97:27-33.

[48] Swadźba R, Marugi K, Pyclik. STEM investigations of γ-TiAl produced by additive manufacturing after isothermal oxidation. Corros Sci. 2020 Jun 1;169:108617.

[49] Bacos MP, Thomas M, Raviart JL, Morel A, Mercier S, Josso P. Influence of an oxidation protective coating upon hot corrosion and mechanical behaviour of Ti-48Al-2Cr-2Nb alloy. Intermetallics. 2011 Aug 1;19(8):1120-1129.

[50] Mitoraj-Królikowska M, Godlewska E. Hot corrosion behaviour of (γ + α2)-Ti-46Al-8Nb (at.%) and α-Ti-6Al-1Mn (at.%) alloys. Corros Sci. 2017 Feb 1;115:18-29.

[51] Godlewska E, Mitoraj M, Leszczynska K. Hot corrosion of Ti-46Al-8Ta (at.%) intermetallic alloy. Corros Sci. 2014 Jan 1;78:63-70.

[52] Qu SJ, Tang SQ, Feng AH, Feng C, Shen J, Chen DL. Microstructural evolution and high-temperature oxidation mechanisms of a titanium aluminide based alloy [Internet]. Vol. 148, Acta Materialia. 2018. p. 300-10. Available from: http://www.sciencedirect.com/science/article/pii/S1359645418301149

[53] Maliutina IN, Si-Mohand H, Sijobert J, Bertrand P, Lazurenko D V., Bataev IA. Structure and oxidation behavior of γ-TiAl coating produced by laser cladding on titanium alloy. Surf Coatings Technol. 2017 Jun 15;319:136-144.

[54] Kothari K, Radhakrishnan R, Wereley NM. Advances in gamma titanium aluminides and their manufacturing techniques. Prog Aerosp Sci. 2012;55:1-16.

[55] Huang SC, Chesnutt JC. Intermetallic Compounds. Principles and Practice, Vol. 2 Practice: Gamma TiAl and its Alloys. 1995;

[56] Mogale NF, Matizamhuka WR. Spark Plasma Sintering of Titanium Aluminides: A Progress Review on Processing, Structure-Property Relations, Alloy Development and Challenges. Metals (Basel) [Internet]. 2020 Aug 11 [cited 2021 Apr 20];10(8):1080. Available from: https://www.mdpi.com/2075-4701/10/8/1080

[57] Cobbinah P V, Matizamhuka WR. Solid-State Processing Route, Mechanical Behaviour, and Oxidation Resistance of TiAl Alloys. Adv Mater Sci Eng. 2019;2019.

[58] Ding J, Zhang M, Liang Y, Ren Y, Dong C, Lin J. Enhanced high-temperature tensile property by gradient twin structure of duplex high-Nb-containing TiAl alloy. Acta Mater. 2018 Dec 1;161:1-11.

[59] Appel F, Paul JDH, Oehring M. Gamma titanium aluminide alloys: science and technology. John Wiley & Sons; 2011.

[60] Yamaguchi M, Inui H, Ito K. High-temperature structural intermetallics [Internet]. Vol. 48, Acta Materialia. 2000. p. 307-22. Available from: http://www.sciencedirect.com/science/article/pii/S1359645499003018

[61] Clemens H, Mayer S. Design, Processing, Microstructure, Properties,

and Applications of Advanced Intermetallic TiAl Alloys. Adv Eng Mater [Internet]. 2013;15(4):191-215. Available from: https://doi.org/10.1002/adem.201200231

[62] Wimler D, Kardos S, Lindemann J, Clemens H, Mayer S. Aspects of Powder Characterization for Additive Manufacturing. Pract Metallogr [Internet]. 2018;55(9):620-36. Available from: https://doi.org/10.3139/147.110547

[63] Schimbäck D, Braun J, Leichtfried G, Clemens H, Mayer S. Laser powder bed fusion of an engineering intermetallic TiAl alloy. Mater Des. 2021 Mar 1;201:109506.

[64] Clemens H, Mayer S. Intermetallic titanium aluminides in aerospace applications—Processing, microstructure and properties. Mater High Temp [Internet]. 2016;33(4):560-570. Available from: http://search.ebscohost.com/login.aspx?direct=true&db=a9h&AN=118805116&site=eds-live

[65] Löber L, Biamino S, Ackelid U, Sabbadini S, Epicoco P, Fino P, et al. Comparison of selective laser and electron beam melted titanium aluminides. In: Conference paper of 22nd International symposium "Solid freeform fabrication proceedings", University of Texas, Austin. 2011. p. 547-556.

[66] Thomas M, Malot T, Aubry P, Colin C, Vilaro T, Bertrand P. The prospects for additive manufacturing of bulk TiAl alloy. Mater High Temp [Internet]. 2016 Jun 28;33(4-5):571-7. Available from: https://doi.org/10.1080/09603409.2016.1171510

[67] Zhang X, Mao B, Mushongera L, Kundin J, Liao Y. Laser powder bed fusion of titanium aluminides: An investigation on site-specific microstructure evolution mechanism. Mater Des. 2021 Mar 1;201:109501.

[68] Li W, Liu J, Zhou Y, Li S, Wen S, Wei Q, et al. Effect of laser scanning speed on a Ti-45Al-2Cr-5Nb alloy processed by selective laser melting: Microstructure, phase and mechanical properties. J Alloys Compd. 2016 Dec 15;688:626-636.

[69] Caprio L, Demir AG, Chiari G, Previtali B. Defect-free laser powder bed fusion of Ti–48Al–2Cr–2Nb with a high temperature inductive preheating system. J Phys Photonics [Internet]. 2020 Feb 12;2(2):024001. Available from: https://iopscience.iop.org/article/10.1088/2515-7647/ab7080

[70] Shi X, Wang H, Feng W, Zhang Y, Ma S, Wei J. The crack and pore formation mechanism of Ti–47Al–2Cr–2Nb alloy fabricated by selective laser melting. Int J Refract Met Hard Mater. 2020 Sep 1;91:105247.

[71] Gussone J, Hagedorn YC, Gherekhloo H, Kasperovich G, Merzouk T, Hausmann J. Microstructure of γ-titanium aluminide processed by selected laser melting at elevated temperatures. Intermetallics. 2015 Jul 21;66:133-140.

[72] Sola A, Nouri A. Microstructural porosity in additive manufacturing: The formation and detection of pores in metal parts fabricated by powder bed fusion. J Adv Manuf Process [Internet]. 2019 Jul 1;1(3):e10021. Available from: https://doi.org/10.1002/amp2.10021.

[73] Abdulrahman KO, Akinlabi ET, Mahamood RM, Pityana S, Tlotleng M. Laser metal deposition of titanium aluminide composites: A review. In: Materials Today: Proceedings. Elsevier Ltd; 2018. p. 19738-19746.

[74] Cobbinah PV, Nzeukou RA, Onawale OT, Matizamhuka WR. Laser Powder Bed Fusion of Potential Superalloys: A Review. Metals (Basel). 2021;11(1):58.

[75] Polozov I, Kantyukov A, Popovich V, Zhu JN, Popovich A. Microstructure and mechanical properties of tial-based alloy produced by selective laser melting. In: METAL 2020—29th International Conference on Metallurgy and Materials, Conference Proceedings [Internet]. TANGER Ltd.; 2020 [cited 2021 May 3]. p. 1037-41. Available from: https://doi.org/10.37904/metal.2020.3604

[76] Gao P, Wang Z. Formability improvement, cracking behavior and control of Y-modified Ti–43Al–4Nb–1Mo-0.1B alloys produced by selective laser melting. J Alloys Compd. 2021 Feb 15;854:157172.

[77] Ismaeel A, Wang C. Effect of Nb additions on microstructure and properties of γ-TiAl based alloys fabricated by selective laser melting. Trans Nonferrous Met Soc China. 2019;29(5):1007-1016.

[78] Mahajan S, Chhibber R. Hot corrosion studies of boiler steels exposed to different molten salt mixtures at 950°C. Eng Fail Anal. 2019 May 1;99:210-224.

[79] Prashar G, Vasudev H. Hot corrosion behavior of super alloys. 2020; Available from: https://doi.org/10.1016/j.matpr.2020.02.226

[80] Zhang W-J, Sharghi-Moshtaghin R. Revisit the Type II Corrosion Mechanism. Available from: https://doi.org/10.1007/s11661-018-4755-4

[81] Kumar S, Kumar M, Handa A. Combating hot corrosion of boiler tubes—A study. Vol. 94, Engineering Failure Analysis. Elsevier Ltd; 2018. p. 379-395.

[82] Liu YD, Sun J, Pei ZL, Li W, Liu JH, Gong J, et al. Oxidation and hot corrosion behavior of NiCrAlYSi+NiAl/cBN abrasive coating. Corros Sci. 2020 May 1;167:108486.

[83] He DG, Lin YC, Tang Y, Li L, Chen J, Chen MS, et al. Influences of solution cooling on microstructures, mechanical properties and hot corrosion resistance of a nickel-based superalloy. Mater Sci Eng A. 2019 Feb 11;746:372-383.

[84] Naghiyan Fesharaki M, Shoja-Razavi R, Mansouri HA, Jamali H. Evaluation of the hot corrosion behavior of Inconel 625 coatings on the Inconel 738 substrate by laser and TIG cladding techniques. Opt Laser Technol. 2019 Apr 1;111:744-753.

[85] Smialek JL, Nesbitt JA, Gabb TP, Garg A, Miller RA. Hot corrosion and low cycle fatigue of a Cr2AlC-coated superalloy. Mater Sci Eng A. 2018 Jan 10;711:119-129.

[86] HU Y tao, ZHENG L, YAN H jie, WU L kui, LIN X jun, CAO F he, et al. Improving hot corrosion resistance of aluminized TiAl alloy by anodization and pre-oxidation. Trans Nonferrous Met Soc China (English Ed. 2021 Jan 1;31(1):193-206.

[87] Garip Y, Ozdemir O. Corrosion behavior of the resistance sintered TiAl based intermetallics induced by two different molten salt mixture. Corros Sci. 2020 Sep 1;174:108819.

[88] Chang JX, Wang D, Zhang G, Lou LH, Zhang J. Interaction of Ta and Cr on Type-I hot corrosion resistance of single crystal Ni-base superalloys. Corros Sci. 2017 Mar 1;117:35-42.

[89] Cockings HL, Cockings BJ, Harrison W, Dowd M, Perkins KM, Whittaker MT, et al. The effect of near-surface plastic deformation on the hot corrosion and high temperature corrosion-fatigue response of a nickel-based superalloy. J Alloys Compd. 2020 Aug 15;832:154889.

[90] Nabavi B, Goodarzi M, Khan AK. Metallurgical effects of nitrogen on the microstructure and hot corrosion

behavior of Alloy 718 weldment. Mater Charact. 2019 Nov 1;157:109916.

[91] Aung NN, Liu X. Effect of SO2 in flue gas on coal ash hot corrosion of Inconel 740 alloy—A high temperature electrochemical sensor study. Corros Sci. 2013 Nov 1;76:390-402.

[92] Patel NS, Pavlík V, Boča M, Bo M. Critical Reviews in Solid State and Materials Sciences High-Temperature Corrosion Behavior of Superalloys in Molten Salts-A Review High-Temperature Corrosion Behavior of Superalloys in Molten Salts-A Review. 2016; Available from: https://www. tandfonline.com/action/journalInforma tion?journalCode=bsms20

[93] Nicholls JR, Simms NJ. Gas turbine oxidation and corrosion. In: Shreir's Corrosion. Elsevier; 2010. p. 518-540.

[94] Eliaz N, Shemesh G, Latanision RM. Hot corrosion in gas turbine components. Eng Fail Anal. 2002 Feb 1;9(1):31-43.

[95] Sulfidation: Turbine Blade Corrosion | Aviation Pros [Internet]. [cited 2021 Apr 14]. Available from: https://www.aviationpros.com/engines-components/aircraft-engines/turbine-engine-maintenance/article/10378159/sulfidation-turbine-blade-corrosion

[96] Part II: Corrosion Topics. In: Corrosion Atlas Case Studies. Elsevier; 2020. p. xliii–lxviii.

[97] Pettit F. Hot corrosion of metals and alloys [Internet]. Vol. 76, Oxidation of Metals. Springer; 2011 [cited 2021 Apr 15]. p. 1-21. Available from: https://link. springer.com/article/10.1007/s11085-011-9254-6

[98] LUTHRA KL. LOW TEMPERATURE HOT CORROSION OF COBALT-BASE ALLOYS—1. MORPHOLOGY OF THE REACTION PRODUCT. Met TRANS A [Internet].

1982 [cited 2021 Apr 15];13(N 10):1843-52. Available from: https://link.springer. com/article/10.1007/BF02647841

[99] LUTHRA KL. LOW TEMPERATURE HOT CORROSION OF COBALT-BASE ALLOYS—2. REACTION MECHANISM. Met TRANS A. 1982;13(N 10):1853-1864.

[100] Lutz BS, Alvarado-Orozco J M, Garcia-Fresnillo L, Meier GH. Na2SO4-Deposit-Induced Corrosion of Mo-Containing Alloys. Present Address AUTOVISION Serv. 2017;88:599-620.

[101] Alvarado-Orozco JM, Garcia-Herrera J E, Gleeson B, Pettit F S, Meier G H, Meier GH. Reinterpretation of Type II Hot Corrosion of Co-Base Alloys Incorporating Synergistic Fluxing. Oxid Met [Internet]. 2018;90:527-53. Available from: https://doi.org/10.1007/s11085-018-9853-6

[102] Gheno T, Gleeson B. On the Hot Corrosion of Nickel at 700°C. Oxid Met. 84.

[103] Sumner J, Encinas-Oropesa A, Simms NJ, Nicholls JR. Type II Hot Corrosion: Kinetics Studies of CMSX-4.

[104] Haight H, Potter A, Sumner J, Gray S. New Technique to Map Hot Corrosion Damage: CMSX-4 Example.

[105] Lortrakul P, Trice RW, Trumble KP, Dayananda MA. Investigation of the mechanisms of Type-II hot corrosion of superalloy CMSX-4. Corros Sci. 2014 Mar 1;80:408-415.

[106] Lillerud KP, Kofstad P. Sulfate-Induced Hot Corrosion of Nickel. Vol. 21, Oxidation of Metals. 1984.

[107] Alizadeh M, Izadi A, Fathi A. Sensitivity Analysis on Turbine Blade Temperature Distribution Using Conjugate Heat Transfer Simulation. J Turbomach [Internet]. 2013 Sep 20;136(1). Available from: https://doi. org/10.1115/1.4024637

[108] Taamneh Y. Thermal analysis of gas turbine disk integrated with rotating heat pipes. Case Stud Therm Eng. 2017 Sep 1;10:335-342.

[109] Goebel JA, Pettit FS. Na2SO4-1nduced Accelerated Oxidation (Hot Corrosion) of Nickel.

[110] Goebel JA, Pettit FS. The Influence of Sulfides on the Oxidation Behavior of Nickel-Base Alloys.

[111] Luthra KL. Mechanism of low temperature hot corrosion. High Temp Corros. 1983;507-512.

[112] Shih S, Zhang Y, Li X. Sub-melting point hot corrosion of alloys and coatings. Mater Sci Eng A. 1989 Nov 15;120-121(PART 1):277-82.

[113] Otsuka N, Rapp RA. Hot Corrosion of Preoxidized Ni by a Thin Fused Na2SO4 Film at 900°C. J Electrochem Soc [Internet]. 1990 Jan 1;137(1):46-52. Available from: https://iopscience.iop.org/article/10.1149/1.2086436

[114] Zhang K, Li Z, Gao W. Hot corrosion behaviour of Ti-Al based intermetallics. Mater Lett. 2002 Dec 1;57(4):834-843.

[115] Tang Z, Wang F, Wu W. Effect of a sputtered TiAlCr coating on hot corrosion resistance of gamma-TiAl. Intermetallics. 1999 Nov 1;7(11):1271-1274.

[116] Tang Z, Wang F, Wu W. Effect of Al2O3 and enamel coatings on 900°C oxidation and hot corrosion behaviors of gamma-TiAl. Mater Sci Eng A. 2000 Jan 15;276(1-2):70-75.

[117] Nicholls JR, Saunders SRJ. Comparison of hot-salt corrosion behaviour of superalloys in high and low velocity burner rigs. High Temp Technol [Internet]. 1989 [cited 2021 Apr 19];7(4):193-201. Available from: https://www.tandfonline.com/doi/abs/10.1080/02619180.1989.11753437

[118] Lai GY, Barnes JJ, Barnes JE. A Burner Rig Investigation of the Hot Corrosion Behavior of Several Wrought Superalloys and Intermetallics [Internet]. 1991. Available from: https://doi.org/10.1115/91-GT-021

[119] Knutsson P, Lai H, Stiller K. A method for investigation of hot corrosion by gaseous Na2SO4. Corros Sci. 2013 Aug 1;73:230-236.

[120] SIMONS EL, BROWNING G V, LIEBHAFSKY HA. Sodium Sulfate in Gas Turbines★. Corrosion [Internet]. 1955 Dec 1;11(12):17-26. Available from: https://doi.org/10.5006/0010-9312-11.12.17

[121] Stringer J. High-temperature corrosion of superalloys. Mater Sci Technol [Internet]. 1987 Jul 1;3(7):482-93. Available from: https://doi.org/10.1080/02670836.1987.11782259

[122] Hancock PJ, Hancock HA, Caley WF, Hollingshead RS. A review of recent studies of the role of zinc as an inhibitor of hot corrosion from molten sulphates. Mater Sci Eng A. 1989 Nov 15;120-121(PART 1):313-8.

[123] Otsuka N, Rapp RA. Effects of Chromate and Vanadate Anions on the Hot Corrosion of Preoxidized Ni by a Thin Fused Na2SO4 Film at 900°C. J Electrochem Soc [Internet]. 1990 Jan 1;137(1):53-60. Available from: https://iopscience.iop.org/article/10.1149/1.2086437

[124] Gurrappa I. Hot Corrosion Behavior of CM 247 LC Alloy in Na2SO4 and NaCl Environments. Vol. 51, Oxidation of Metals. 1999.

[125] Garip Y, Ozdemir O. Corrosion behavior of the resistance sintered TiAl based intermetallics induced by two different molten salt mixture. Corros Sci. 2020 Sep 1;174:108819.

[126] Bornstein NS, DeCrescente MA, Roth HA. The relationship between

relative oxide ion content of Na 2 SO 4, the presence of liquid metal oxides and sulfidation attack. Metall Trans. 1973;4(8):1799-1810.

[127] Nicholls JR. Designing oxidation-resistant coatings. JoM. 2000;52(1):28-35.

[128] Shen M, Zhu S, Wang F. Formation kinetics of multi-layered interfacial zone between γ-TiAl and glass–ceramic coatings via interfacial reactions at 1000°C. Corros Sci. 2015 Feb 1;91:341-351.

[129] Liao Y, Zhang B, Chen M, Feng M, Wang J, Zhu S, et al. Self-healing metal-enamel composite coating and its protection for TiAl alloy against oxidation under thermal shock in NaCl solution. Corros Sci. 2020 May 1;167:108526.

[130] Pflumm R, Friedle S, Schütze M. Oxidation protection of γ-TiAl-based alloys—A review [Internet]. Vol. 56, Intermetallics. 2015. p. 1-14. Available from: http://www.sciencedirect.com/science/article/pii/S0966979514002325

[131] Laska N, Braun R, Knittel S. Oxidation behavior of protective Ti-Al-Cr based coatings applied on the γ-TiAl alloys Ti-48-2-2 and TNM-B1. Surf Coatings Technol. 2018 Sep 15;349:347-356.

[132] Liu XB, Wang HM. Modification of tribology and high-temperature behavior of Ti–48Al–2Cr–2Nb intermetallic alloy by laser cladding. Appl Surf Sci. 2006 Jun 15;252(16):5735-5744.

[133] Gao J, He Y, Gao W. Electro-codeposition of Al2O3–Y2O3 composite thin film coatings and their high-temperature oxidation resistance on γ-TiAl alloy. Thin Solid Films. 2012 Jan 1;520(6):2060-2065.

[134] Xiang ZD, Rose SR, Datta PK. Codeposition of Al and Si to form

oxidation-resistant coatings on γ-TiAl by the pack cementation process. Mater Chem Phys. 2003 May 26;80(2):482-489.

[135] Liang W, Ma XX, Zhao XG, Zhang F, Shi JY, Zhang J. Oxidation kinetics of the pack siliconized TiAl-based alloy and microstructure evolution of the coating. Intermetallics. 2007 Jan 1;15(1):1-8.

[136] Goral M, Swadzba L, Moskal G, Hetmanczyk M, Tetsui T. Si-modified aluminide coatings deposited on Ti46Al7Nb alloy by slurry method. Intermetallics. 2009 Nov 1;17(11):965-967.

[137] Donchev A, Richter E, Schütze M, Yankov R. Improvement of the oxidation behaviour of TiAl-alloys by treatment with halogens. Intermetallics. 2006 Oct 1;14(10-11):1168-1174.

[138] Nakamori M, Kayano I, Tsukuda Y, Takahashi K, Torigoe T. Hot corrosion and its prevention in high temperature heavy oil firing gas turbines. In: Materials science forum. Trans Tech Publ; 1997. p. 633-640.

[139] Güther V, Allen M, Klose J, Clemens H. Metallurgical processing of titanium aluminides on industrial scale. Intermetallics. 2018 Dec 1;103: 12-22.

[140] Wimler D, Lindemann J, Reith M, Kirchner A, Allen M, Vargas WG, et al. Designing advanced intermetallic titanium aluminide alloys for additive manufacturing. Intermetallics. 2021 Apr 1;131:107109.

[141] Polozov I, Popovich V, Razumov N, Makhmutov T, Popovich *A. Gamma*-Titanium Intermetallic Alloy Produced by Selective Laser Melting Using Mechanically Alloyed and Plasma Spheroidized Powders. In: TMS 2020 149th Annual Meeting & Exhibition Supplemental Proceedings. Springer; 2020. p. 375-383.

[142] Polozov I, Sufiiarov V, Kantyukov A, Razumov N, Goncharov I, Makhmutov T, et al. Microstructure, densification, and mechanical properties of titanium intermetallic alloy manufactured by laser powder bed fusion additive manufacturing with high-temperature preheating using gas atomized and mechanically alloyed plasma spheroidized powders. Addit Manuf. 2020 Aug 1;34:101374.

[143] Polozov I, Sufiiarov V, Kantyukov A, Popovich A. Selective Laser Melting of Ti2AlNb-based intermetallic alloy using elemental powders: Effect of process parameters and post-treatment on microstructure, composition, and properties. Intermetallics. 2019 Sep 1;112:106554.

[144] Sizova I, Sviridov A, Bambach M, Eisentraut M, Hemes S, Hecht U, et al. A study on hot-working as alternative post-processing method for titanium aluminides built by laser powder bed fusion and electron beam melting. J Mater Process Technol. 2021 May 1;291:117024.

[145] Reith M, Franke M, Schloffer M, Körner C. Processing 4th generation titanium aluminides via electron beam based additive manufacturing— Characterization of microstructure and mechanical properties. Materialia. 2020 Dec 1;14:100902.

[146] Gasper AND, Catchpole-Smith S, Clare AT. In-situ synthesis of titanium aluminides by direct metal deposition. J Mater Process Technol. 2017 Jan 1;239:230-239.

[147] Garip Y, Ozdemir O. Comparative study of the oxidation and hot corrosion behaviors of TiAl-Cr intermetallic alloy produced by electric current activated sintering. J Alloys Compd. 2019 Apr 5;780:364-377.

[148] Dai J, Zhang H, Sun C, Li S, Chen C, Yang Y. The effect of Nb and Si on the hot corrosion behaviors of TiAl coatings on a Ti-6Al-4V alloy. Corros Sci. 2020 May 15;168:108578.

[149] Tang Z, Wang F, Wu W. Effect of Al2O3 and enamel coatings on 900°C oxidation and hot corrosion behaviors of gamma-TiAl. Mater Sci Eng A. 2000 Jan 15;276(1-2):70-75.

[150] Rubacha K, Godlewska E, Mars K. Behaviour of a silicon-rich coating on Ti-46Al-8Ta (at.%) in hot-corrosion environments. Corros Sci. 2017 Apr 1;118:158-167.

[151] Wu LK, Wu JJ, Wu WY, Yan HJ, Jiang MY, Cao FH. Hot corrosion behavior of electrodeposited SiO2 coating on TiAl alloy. Corros Sci. 2020 Sep 1;174:108827.

[152] Swadźba R, Swadźba L, Mendala B, Witala B, Tracz J, Marugi K, et al. Characterization of Si-aluminide coating and oxide scale microstructure formed on γ-TiAl alloy during long-term oxidation at 950°C. Intermetallics. 2017 Aug 1;87:81-89.

[153] Lim HP, Yun W, Liew H, Jet G, Melvin H, Jiang Z-T, et al. materials A Short Review on the Phase Structures, Oxidation Kinetics, and Mechanical Properties of Complex Ti-Al Alloys. 2021; Available from: https://doi.org/10.3390/ma14071677

[154] Samal S. High-Temperature Oxidation of Metals. In: High Temperature Corrosion [Internet]. InTech; 2016 [cited 2021 Apr 21]. Available from: http://dx.doi.org/10.5772/63000

[155] Cobbinah PV, Matizamhuka W, Machaka R, Shongwe MB, Yamabe-Mitarai Y. The effect of Ta additions on the oxidation resistance of SPS-produced TiAl alloys. Int J Adv Manuf Technol. 2020;106(7-8):3203-3215.

[156] Pan Y, Lu X, Hayat MD, Yang F, Liu CC, Li Y, et al. Effect of Sn addition on the high-temperature oxidation behavior of high Nb-containing TiAl alloys. Corros Sci. 2020 Apr 15;166:108449.

[157] Wu LK, Wu WY, Song JL, Hou GY, Cao HZ, Tang YP, et al. Enhanced high temperature oxidation resistance for γ-TiAl alloy with electrodeposited SiO2 film. Corros Sci. 2018 Aug 1;140:388-401.

[158] Friedle S, Pflumm R, Seyeux A, Marcus P, Schü Tze M. ToF-SIMS Study on the Initial Stages of the Halogen Effect in the Oxidation of TiAl Alloys. Available from: https://doi.org/10.1007/s11085-017-9779-4

[159] Mo MH, Wu LK, Cao HZ, Lin JP, Zheng GQ. Halogen effect for improving high temperature oxidation resistance of Ti-50Al by anodization. Appl Surf Sci. 2017 Jun 15;407: 246-254.

[160] Mo M, Wu L, Cao H, Lin J, Zheng G. Improvement of the high temperature oxidation resistance of Ti–50Al at 1000°C by anodizing in ethylene glycol/BmimPF6 solution. Surf Coatings Technol. 2016 Jan 25;286:215-222.

[161] Wu LK, Xia JJ, Jiang MY, Wang Q, Wu HX, Sun DB, et al. Oxidation behavior of Ti45Al8.5Nb alloy anodized in NH4F containing solution. Corros Sci. 2020 Apr 15;166:108447.

[162] Wu L-K, Xia J-J, Cao H-Z, Liu W-J, Guang-Ya Hou ·, Tang Y-P, et al. Improving the High-Temperature Oxidation Resistance of TiAl Alloy by Anodizing in Methanol/NaF Solution. 2018;90:617-31. Available from: https://doi.org/10.1007/s11085-018-9858-1

[163] Appel F, David J, Paul H, Oehring *M. Gamma* Titanium Aluminide Alloys.

[164] Garip Y. Investigation of isothermal oxidation performance of TiAl alloys sintered by different processing methods. Intermetallics. 2020 Dec 1;127:106985.

[165] Dai J, Zhu J, Chen C, Weng F. High temperature oxidation behavior and research status of modifications on improving high temperature oxidation resistance of titanium alloys and titanium aluminides: A review [Internet]. Vol. 685, Journal of Alloys and Compounds. 2016. p. 784-98. Available from: http://www.sciencedirect.com/science/article/pii/S0925838816319351

[166] Raji SA, Popoola API, Pityana SL, Popoola OM. Characteristic effects of alloying elements on β solidifying titanium aluminides: A review. Vol. 6, Heliyon. Elsevier Ltd; 2020. p. e04463.

[167] Kothari K, Radhakrishnan R, Wereley NM, Sudarshan TS. Microstructure and mechanical properties of consolidated gamma titanium aluminides. Powder Metall. 2007;50(1):21-27.

[168] JIANG H ren, WANG Z lei, MA W shuai, FENG X ran, DONG Z qiang, ZHANG L, et al. Effects of Nb and Si on high temperature oxidation of TiAl. Trans Nonferrous Met Soc China (English Ed. 2008 Jun 1;18(3):512-7.

[169] Pflumm R, Donchev A, Mayer S, Clemens H, Schütze M. High-temperature oxidation behavior of multi-phase Mo-containing γ-TiAl-based alloys. Intermetallics. 2014 Oct 1;53:45-55.

[170] Wei DB, Zhang PZ, Yao ZJ, Liang WP, Miao Q, Xu Z. Oxidation of double-glow plasma chromising coating on TC4 titanium alloys. Corros Sci. 2013 Jan 1;66:43-50.

[171] Zhou C, Yang Y, Gong S, Xu H. Mechanism of Cr effect for improvement of oxidation resistance of

Ti-Al-Cr alloys. Acta Aeronaut Asronautica Sin. 2001;22(1):73-77.

[172] Gaddam R, Sefer B, Pederson R, Antti ML. Oxidation and alpha-case formation in Ti-6Al-2Sn-4Zr-2Mo alloy. Mater Charact. 2015 Jan 1;99:166-174.